J. Fluid Mech. (1979), *vol.* 94, *part* 3, *pp.* 577–594
Printed in Great Britain

Streamwise vortices associated with the bursting phenomenon

By RON F. BLACKWELDER

Department of Aerospace Engineering, University of Southern California, Los Angeles†

AND HELMUT ECKELMANN

Lehrstuhl für Angewandte Mechanik und Strömungsphysik, University of Göttingen

(Received 21 January 1978 and in revised form 30 October 1978)

The streamwise and spanwise velocity components and the gradients of these components normal to the wall were examined by using hot-film sensors and flush-mounted wall elements to study the vortex structures associated with the bursting phenomenon. Quadrant probability analysis and conditional sampling techniques indicated that pairs of counter-rotating streamwise vortices occur frequently in the wall region of a bounded turbulent shear flow. A streamwise momentum defect occurred between the vortices as low-speed fluid was 'pumped' away from the wall by the vortex pair. The defect region was long and narrow and possibly forms the low-speed streak as observed in visualization studies. The velocity defect was terminated by a strong acceleration followed by a high speed region.

1. Introduction

Research in the past decade of bounded turbulent shear flows has found that the wall region is dominated by a sequence of events which has been called the bursting phenomenon. It is known that this phenomenon is associated with most of the turbulent energy production in this region, and hence in the entire shear flow, and thus is of great importance in the dynamics of the flow field. In visualization studies, this sequence of events is first noticed by the occurrence of low-speed streaks in the streamwise direction. Parts of these streaks lift up away from the wall in an ejection phase, become unstable, oscillate, and break down. This is followed by a sweep of large-scale, high-momentum fluid that originates in the outer flow field and moves at small angles toward the wall. This motion causes a strong mixing with the low-speed outward moving fluid. For further details, reference can be made to the review articles of Willmarth (1975) and Laufer (1975).

The details of the formation of the low-speed streaks is one aspect of this problem which is least understood. Most of the data has been obtained from visualization studies. Hama (see Corrsin 1957) found that by injecting dye at the wall in a turbulent shear flow, low-speed streaks were observed to occur randomly in space and time. Kline & Rundstadler (1959) first studied this motion and speculated that the low-speed streaks were related to an organized three-dimensional vortical structure in the

† This research was performed while at the Max-Planck-Institut für Strömungsforschung, Göttingen.

0022–1120/79/4288–7340 $02.00

wall layer. Kline *et al.* (1967) confirmed these ideas in a further study using hydrogen bubble wires in addition to dye injection. Corino & Brodkey (1969) used neutrally buoyant particles and found the wall region strongly affected by the high speed fluid associated with the outer flow field. They and Kim, Kline & Reynolds (1971) showed that most of the turbulent production of energy was due to the organized motion. More recently, Oldaker & Tiederman (1977) utilized a fluorescent dye with different lighting techniques in order to further explore the same phenomenon. These and other studies have indicated that the low-speed streaks are a precursor to and an important part of the bursting phenomenon; however, the mechanism responsible for their origin is not clear.

Grant (1958) obtained some of the earliest data from hot-wire anemometers that pertained to this structure. Townsend (1970) showed that Grant's spatial correlations were consistent with a narrow two-dimensional jet-like flow in the wall region. Bakewell & Lumley (1967) used a set of space–time correlations in the wall region of a pipe flow together with an orthogonal decomposition theorem and found that the velocities were consistent with a pair of counter-rotating streamwise vortices. Gupta, Laufer & Kaplan (1971) used a rake of hot wires in the spanwise direction and found alternating regions of high- and low-speed streamwise momentum. They further showed that the wavelength in the spanwise direction was a random variable and that long-time correlations eliminated most evidence of this structure. Lee, Eckelmann & Hanratty (1974) used electrochemical probes flush-mounted on the wall and observed a similar pattern. All of these data suggest that the system of counter-rotating streamwise vortices probably exists in the wall region of bounded turbulent shear flows but occur randomly in space and time. The mean values of the wavelength and height could be measured in principle; however, these parameters are also random variables. This research was undertaken to determine if such a system of vortices could be instantaneously detected by using probe techniques and whether they could be responsible for the low-speed streaks.

2. Experimental techniques

Because the wall region in bounded turbulent shear flows has very small spatial scales, considerable experimental difficulties are encountered in attempting to study its structure. Any sensor that can be used in this region usually has a size greater than the characteristic length scale of the viscous sublayer which can cause probe interference. Although a laser-Doppler anemometer may be considered ideal, it is quite cumbersome and has resolution difficulties near the wall. Since the spatial structure occurs randomly in space and time, multi-point sensors must be used to measure anything more complicated than the simple common length scales. The solution employed in this investigation was to use heated wall elements. These are flat hot-films that are flush-mounted on the wall and hence do not cause any physical probe interference. The wall elements were DISA type 55A93 sensors which are 0·75 mm long and 0·15 mm wide. When aligned so that their main axis is perpendicular to the mean velocity, the rate of heat transfer from these elements to the fluid is a function of the velocity gradient $(\partial u/\partial y)|_w$. For the measurements reported here, two sensors were used in a pair to form a V-configuration. Analogously to two hot-films arranged in a V-shape, it was assumed that the sum of the two signals was proportional to the

gradient of the streamwise velocity component and that the difference produced a signal proportional to the corresponding spanwise velocity gradient at the wall. Similar V-configurations of electrochemical sensors have been used by Sirkar & Hanratty (1970).

A Taylor series expansion of the streamwise and spanwise velocity components near the wall yields

$$u(y,t) \approx \frac{\partial u(t)}{\partial y}\bigg|_w y$$

and

$$w(y,t) \approx \frac{\partial w(t)}{\partial y}\bigg|_w y.$$

Thus the velocity gradient signals obtained from the wall elements are proportional to the streamwise and spanwise velocity components near the wall. On the other hand, the streamwise and spanwise vorticity components are given by

$$\omega_x = \frac{\partial w}{\partial y} - \frac{\partial v}{\partial z}$$

and

$$\omega_z = \frac{\partial v}{\partial x} - \frac{\partial u}{\partial y}.$$

Using a Taylor expansion, one can show that the streamwise vorticity near the wall equals the gradient of the spanwise velocity component there. Likewise, the spanwise vorticity component at the wall is proportional to the gradient of the streamwise velocity component. Thus the signals proportional to the velocity gradients at the wall can be thought of as a measure of these two vorticity components there. However, this interpretation is only valid near the wall in the linear velocity region, and cannot be used as a measure of the vortex structures occurring further away from the boundary.

The data were all obtained in the oil channel used by Eckelmann (1974). The Reynolds number based upon the channel width was 7700. A part of the test section was a replaced by a special wall that had several pairs of flush-mounted wall elements and was equipped with a removable plug into which special probe configurations and sensors could be placed.

Two different configurations of probes and flush-mounted wall elements were used, as shown in figure 1. Initially measurements were made to determine if consistent evidence of the streamwise vortex structures could be found with the wall elements. These measurements consisted of using two flush-mounted V-probes displaced from each other by Δz^+, as shown in figure 1 (*a*). Although Δz^+ could not be varied continuously, there were a sufficient number of V-probes available so that many different spatial separations could be obtained. Later a single hot-film probe sensitive to the streamwise velocity was placed midway between the two pairs of wall elements at an elevation of $y^+ = 15$. This sensor was used primarily as a detector probe for the bursting phenomenon to obtain the conditional averages. In order to more fully explore the spanwise structure of the bursting phenomenon, the probe configuration shown in figure 1 (*b*) was used. This arrangement consisted of a single velocity probe mounted at $y^+ = 15$ directly above the virtual origin. A V-probe was embedded in the wall at a spanwise distance of z^+ from the origin. At the same spanwise position, a V-configuration of two hot-films was traversed normal to the wall so that the streamwise and

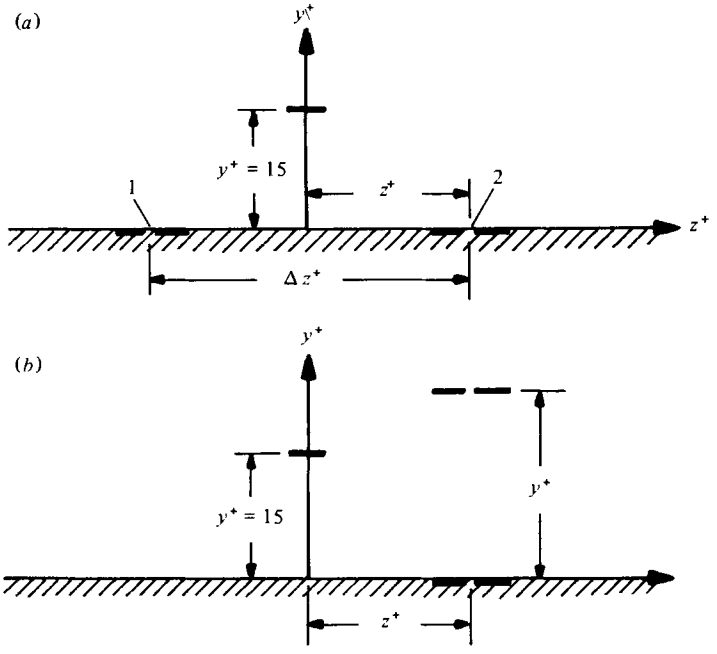

FIGURE 1. Diagram of the probe arrangements. Δz^+ is the distance between the two pairs of wall elements and z^+ is the spanwise position of the wall elements and V-probe. 1 and 2 in (*a*) refer to the subscripts in table 1.

spanwise velocity components could be measured there. The spanwise separation z^+ was constant and equal to either 17 or 34. A three-dimensional sketch of this arrangement is shown in the appendix in figure 11. All sensors were located at the same streamwise location. The velocity probes were made at the Max-Planck-Institut für Strömungsforschung using TSI sensors model 10121-20W. The wall elements and hot-films were driven by DISA 55M10 anemometers and were coupled to DISA 55D10 linearizers. The resistance of the hot-films was maintained at 1 % above their cold value and the overheat of the wall elements was 2 %.

Calibration of the single hot-film in figure 1 (*a*) and the movable V-probe in figure 1 (*b*) was accomplished by towing at variable speeds in the channel with the oil at rest. The fixed streamwise velocity probe at $y^+ = 15$ in figure 1 (*b*) was calibrated in situ by operating the channel at different speeds corresponding to known velocities at the location of the probe. The wall probes were also calibrated in situ by operating the oil channel at three different speeds corresponding to known velocity gradients on the wall. In order to avoid errors due to free convection, the flush-mounted hot-films were calibrated as described by Blackwelder & Eckelmann (1977). The streamwise velocity from the V-probe was obtained by using the sum of the linearized signals from the two probes. Correspondingly, the spanwise velocity component was obtained from the difference. An identical technique was used for the V-configuration of the wall probes. It was impossible to yaw these probes directly during the calibration procedure. Hence the angle between the sensors and the mean flow direction was accurately measured. It was assumed that the effective cooling velocity was given by

$$U_{\text{eff}} = \bar{U}\sqrt{(\cos^2\theta + \epsilon^2 \sin^2\theta)},$$

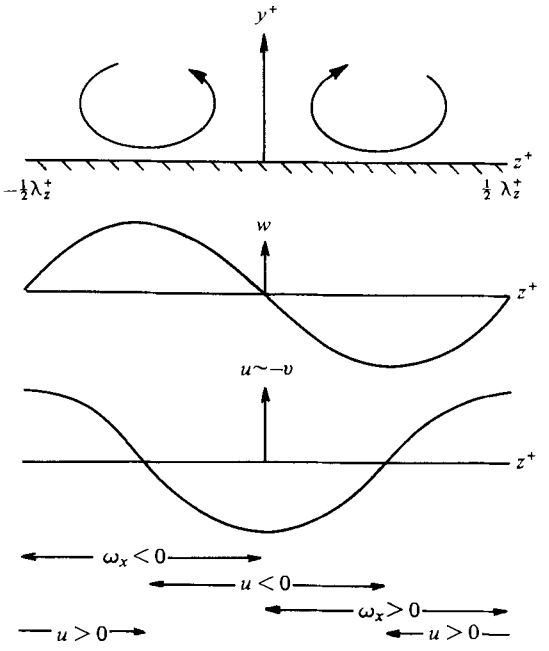

FIGURE 2. End view of an idealized model for a pair of counter-rotating streamwise vortices.

where θ is the angle between the main axis of the sensor and the mean flow, $\overline{U}$. The constant, ϵ, was determined independently by Klages (1977) to be 0·7. With these assumptions, the difference between the signal from the two elements in the V-configuration could reasonably be expected to be proportional to the spanwise velocity. Any remaining systematic errors were checked by calculating the correlation between the streamwise and spanwise velocities, which should be zero by homogeneity. It was typically found that $\overline{uw} < 0{\cdot}1u'w'$. An additional technique was then used which slightly adjusted the calibration slopes of the individual sensors so that $\overline{uw}$ was approximately zero. This adjustment was so small that it lay within the scatter of the calibration data. The calibration was further checked by other symmetry properties that exist in the flow field; such as the antisymmetry of $\overline{uw}(\Delta z^+)$.

All of the calibration data were obtained using analogue techniques in the laboratory. A predetermined constant voltage was subtracted from each of the signals and they were further amplified. These signals were then sent over analogue lines to a multiplexer and an analogue-to-digital converter. The complete system response was tested from d.c. to 10 kHz and was flat within 3 %. The data were digitized and stored on a high-density disk which was controlled by a PDP-15 computer. The magnitude of the bucking voltages and the gains were determined by digitizing known voltages that originated in the laboratory. Further processing of the data was accomplished by FORTRAN programs. At every position each channel was digitized at the rate of 50 samples per second over approximately 30 min giving 90 000 digitized points. This was more than sufficient to guarantee adequate frequency response and statistical reliability.

	1	2	3	4	5	6	7	8	$\bar{8}$	$\bar{7}$	$\bar{6}$	$\bar{5}$	$\bar{4}$	$\bar{3}$	$\bar{2}$	$\bar{1}$
u_1	−	+	−	+	−	+	−	+	−	+	−	+	−	+	−	+
w_1	−	−	+	+	−	−	+	+	−	−	+	+	−	−	+	+
u_2	−	−	−	−	+	+	+	+	−	−	−	−	+	+	+	+
w_2	−	−	−	−	−	−	−	−	+	+	+	+	+	+	+	+

TABLE 1. The 16 different combinations of the four velocity signals.

3. Quadrant analysis of wall element signals

A model of the counterrotating streamwise vortices with a given spanwise scale is shown in figure 2. These vortices are associated with normal and spanwise velocity components that are periodic in the spanwise direction. If this pair exists in a mean flow gradient near the wall, then periodic variations in the streamwise velocity component will also be found. That is, although the streamwise vorticity does not involve u directly, momentum transport due to its motion will cause fluctuations in the streamwise velocity component; for example, between the two vortices shown in figure 2, low-speed fluid will be removed from the wall outward. In this manner, the streamwise velocity acts as a contaminant which gives a measure of the vortex motion. Hence near the wall, the vortex system will produce variations in the velocities as shown.

If two pairs of wall elements separated by Δz^+ are used as shown in figure 1(*a*), signals proportional to the streamwise and spanwise velocity component very near the wall can be obtained at the two locations. At each point in time, the data associated with the four signals can be used to define a single point in a four-dimensional space with each signal corresponding to one axis. If the vortex structures exist, they should inhabit and dominate certain regions of this generalized pattern space as discussed by Blackwelder (1977). The 16 different quadrants in this space correspond to all combinations of the signs of the four signals as shown in table 1. If there is no predominant structure in the wall region, each of these quadrants should be uniformly populated for reasonable Δz^+ separations. On the other hand, if the structure sketched in figure 2 does exist, then there is a higher probability of finding the signals in quadrants 3, 5, $\bar{3}$ and $\bar{5}$ of table 1.

The time spent in each quadrant was computed for ten Δz^+ positions and the results are seen in figure 3. At $\Delta z^+ = 0$, there are only two independent signals, and correspondingly four quadrants (i.e. 1, 6, $\bar{1}$ and $\bar{6}$) are each occupied 25 % of the time. However, the population of these quadrants drops rapidly as Δz^+ increases. At large separations, each quadrant has approximately $\frac{1}{16}$th of the total data as expected. The technique will be most sensitive to the streamwise vortices when the probe separation is $\Delta z^+ \approx \lambda_z^+/4$, as seen in quadrants 3, 5, $\bar{3}$ and $\bar{5}$. As Δz^+ increases from zero, the data lying within each of these quadrants increases rapidly to a peak of approximately 9–14 % at $\Delta z^+ = 20$. The large population increase of these quadrants contrasts that of the other quadrants which evidently are not associated with any coherent structure. Although other coherent eddies could be proposed that would occupy the wall region, it is unlikely that they would produce the results found in figure 3. Note that the time spent in the quadrants corresponding to high- and low-speed streamwise momentum, i.e. quadrants 3 and $\bar{3}$, is significantly larger than that spent in quadrants 5 and $\bar{5}$ associated with only the vortices themselves. Thus it is slightly more probable that

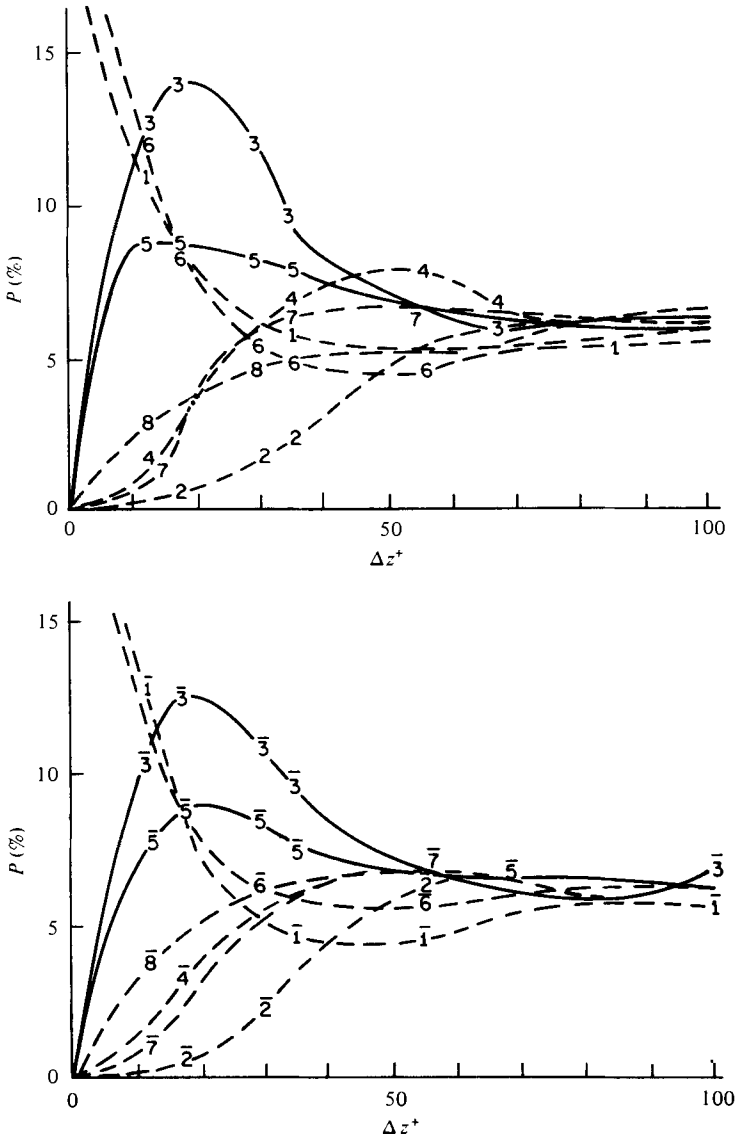

FIGURE 3. Per cent of time spent in each of the sixteen quadrants with eight quadrants shown in each graph. The mnemonic characters represent the data points and correspond to the quadrants in table 1.

one will find a low-speed or high-speed region than a single vortex. This is possibly due to (1) the mutual interaction and evolution of the vortices during their lifetime and/or (2) the disturbances associated with the large scale sweeps which also affect this region.

If the wall region of a bounded shear flow is indeed dominated by pairs of counter-rotating streamwise vortices embedded within random background motions, then the four-dimensional probability density function associated with the pattern space will necessarily contain contributions from the coherent structure as well as the random motion. If the coherent eddies are more energetic than the random fluctuations, their related velocity fluctuations will have excursions further from the origin, and thus a

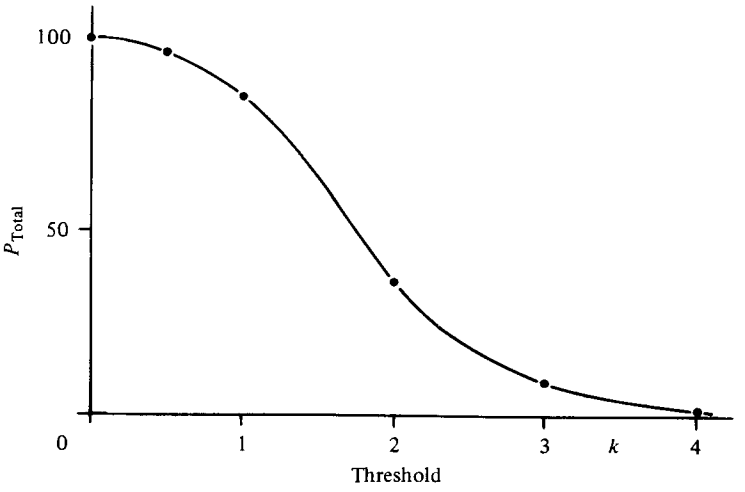

FIGURE 4. Per cent of the total time that the data exceeded the threshold level, k.

threshold can be used to eliminate the non-coherent motions. A characteristic function was defined by

$$f^2(t) = \frac{u_1^2(t)}{\overline{u_1^2}} + \frac{w_1^2(t)}{\overline{w_1^2}} + \frac{u_2^2(t)}{\overline{u_2^2}} + \frac{w_2^2(t)}{\overline{w_2^2}},$$

where $\overline{(\ )^2}$ is the average mean-squared value. This function is a measure of the energy associated with the fluctuations and is equivalent to the Euclidean squared distance from the origin, if the space has been non-dimensionalized with the r.m.s. values. The per cent of time that $f(t)$ exceeded a threshold value, k, is shown in figure 4. As k increased, the amount of data that exceeded the threshold value decreased monotonically. At $k = 4$, almost all of the data lie below the threshold.

Using the above technique, the effects of excluding the random motion from the quadrant analysis was explored. Typical results with $k = 2$ are shown in figure 5 where the ordinate is now the per cent of data in each quadrant that exceeded the threshold. A comparison of figures 3 and 5 shows that the largest differences occur in quadrants 3 and $\bar{3}$; i.e. in the quadrants associated with the low- and high-speed regions lying between the vortices. As the threshold level was increased, the per cent of time spent in quadrants 3 and $\bar{3}$ monotonically increased, suggesting that the coherent structure of these quadrants is associated with the more energetic motions in the wall region.

In a preliminary exploration, the quadrant analysis was used as a detection scheme to find the low-speed regions between counter-rotating streamwise vortices. By using the probe arrangement in figure 1 (*a*) with $\Delta z^+ = 20$, it was found that, when a low-speed region corresponding to quadrant 3 was detected on the wall, a low streamwise velocity usually existed at elevations up to and beyond $y^+ = 15$. The probe at $y^+ = 15$ in figure 1 (*a*) was then replaced by an X-probe and was traversed upstream and downstream of the wall probes. Evidence of an upstream structure or instability mechanism that may be related to or causing the streamwise vortices was sought by using conditional averaging techniques. However, no conclusive evidence of such a mechanism could be found for streamwise probe separations of $\Delta x^+ < 100$. For greater Δx^+

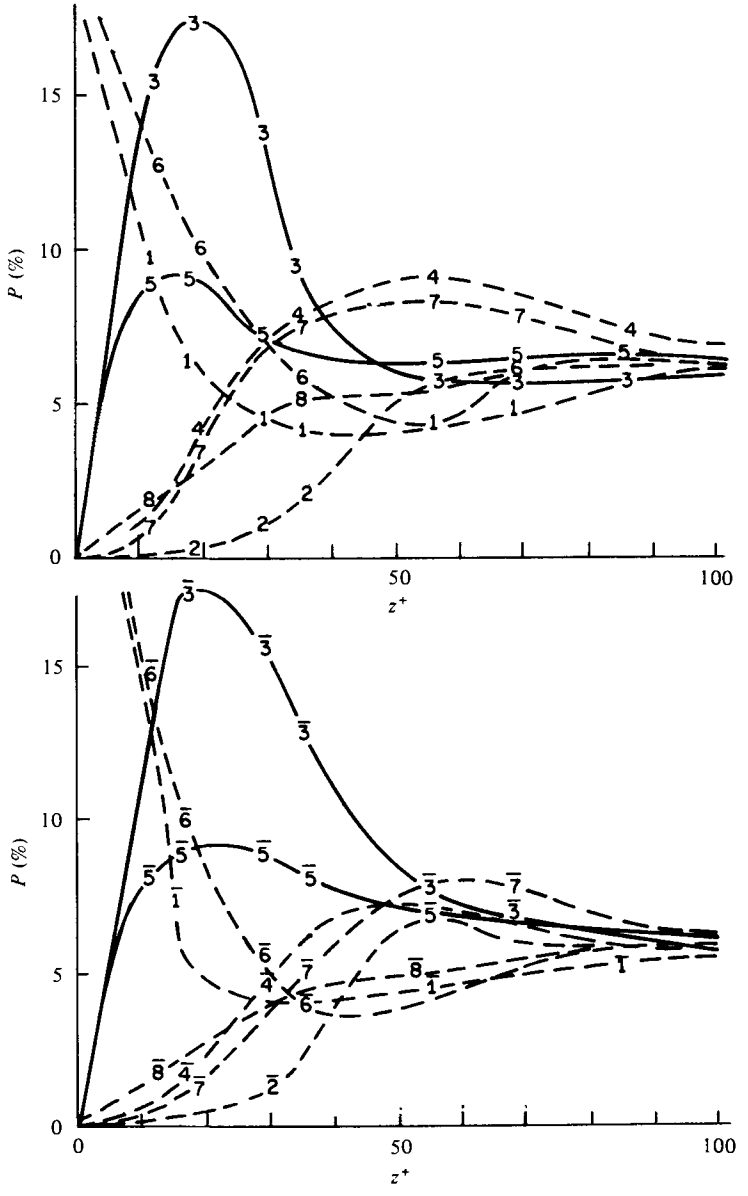

FIGURE 5. Per cent of the time spent in each quadrant for the data that exceeded a threshold level of $k = 2$. The mnemonic characters are the same as used in figure 3 and are given in table 1.

separations, effects of probe interference were found by the methods explained in the appendix. Although no direct evidence of a coherent motion related to the origin of the streamwise vortices was obtained, the detection scheme was quite useful and could be used in the future for such an exploration.

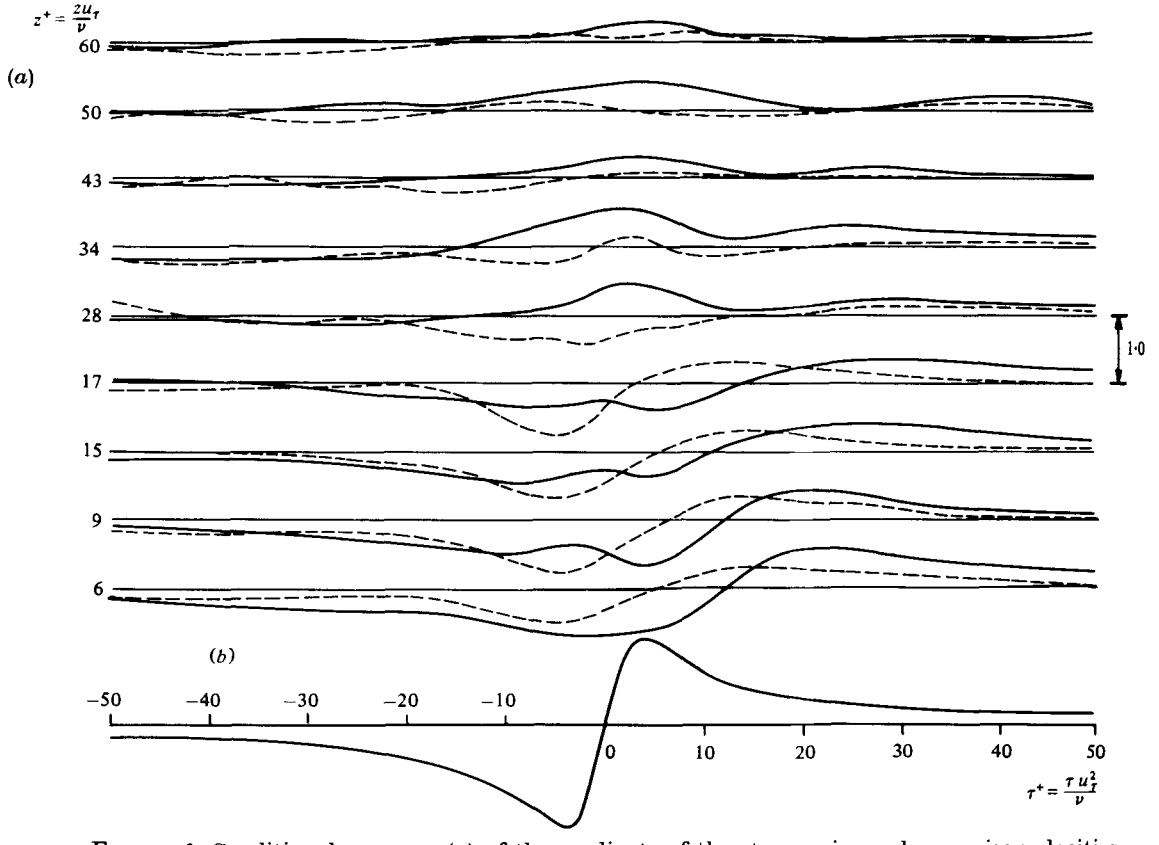

FIGURE 6. Conditional averages (*a*) of the gradients of the streamwise and spanwise velocities on the wall at various spanwise locations and (*b*) of the streamwise velocity at $y^+ = 15$. The probe configuration shown in figure 1 (*a*) was used.

(*a*) ——, $[\langle(du/dy)|_w\rangle - (d\overline{U}/dy)|_w]/[(du/dy)|_w]_{\rm rms}$; – – –, $\langle(dw/dy)|_w\rangle/[(dw/dy)|_w]_{\rm rms}$.

(*b*) $(\langle u(y^+ = 15)\rangle - \overline{U})/u_{\rm rms}$.

4. Conditional averages

The conditional averages of the streamwise and spanwise velocity gradients on the wall obtained with the experimental configuration shown in figure 1 (*a*) were reported by Blackwelder & Eckelmann (1978) and are reproduced in figure 6. The streamwise velocity and velocity gradients are plotted by the solid lines and the spanwise velocity gradients on the wall are given by the dashed lines. Their mean values have been subtracted and they are normalized with their r.m.s. values. The streamwise velocity signal from the probe at $y^+ = 15$ and the detection scheme of Blackwelder & Kaplan (1976) were used to locate the bursts. Their technique utilized a short-time average defined by

$$\hat{u}(t) = \frac{1}{T}\int_{t-\frac{1}{2}T}^{t+\frac{1}{2}T} u(s)\,ds$$

to compute the variance of the streamwise velocity signal, $\widehat{u^2} - \hat{u}^2$ during the interval, T. Their results indicated that statistically significant events related to the bursting

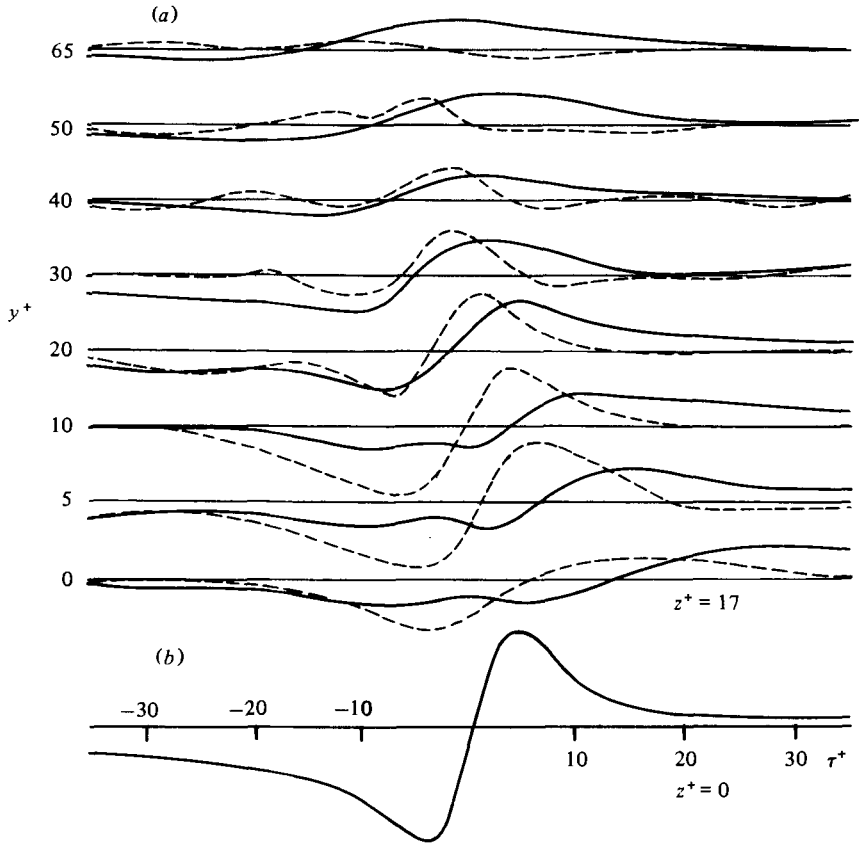

FIGURE 7. Conditional averages of the streamwise and spanwise velocities at $z^+ = 17$ at several y^+ positions from the probe configuration of figure 1(*b*). At $y^+ = 0$ the velocity gradients of figure 6 are shown. (*a*) ——, $(\langle u\rangle - \bar{U})/u_{\rm rms}$; – – –, $\langle w\rangle/w_{\rm rms}$. (*b*) $(\langle u(y^+ = 15)\rangle - \bar{U})/u_{\rm rms}$.

phenomenon occurred whenever the variance exceeded $K.u^2_{\rm rms}$, where K is the threshold parameter. Values of $T^+ = 13$ and $K = 1{\cdot}0$ were used in the present study. The origin of the abscissa in figure 6 corresponds to the detection times and the conditional averages are plotted as a function of the time delay, τ. The velocity scale is given on the right-hand side of the figure. The conditional average of the velocity obtained from the detector probe at $y^+ = 15$ is shown at the bottom of the figure. This result is the same as that found by Blackwelder & Kaplan (1976), confirming that the detection technique works well at diverse Reynolds numbers. The low-speed region at $y^+ = 15$ occurs before the detection scheme is triggered. Directly after an event is detected, i.e. $\tau^+ > 0$, a high-speed velocity associated with the sweep is found. The sharp acceleration arrives later on the wall in agreement with the skewed nature of this sharp velocity front as observed by Kreplin (1976) and by Chen & Blackwelder (1978). Directly before the sweep arrives at the wall locations, the streamwise velocity gradient is less than its mean value for $z^+ < 20$. The strong excess of streamwise momentum seen at $-10 < \tau^+ < 12$ and $z^+ > 20$ may be due to a combination of the sweeps interacting with the higher-speed fluid pumped toward the wall by the vortex motion. Whenever a low-speed region occurred at $y^+ = 15$, the gradient of the spanwise velocity

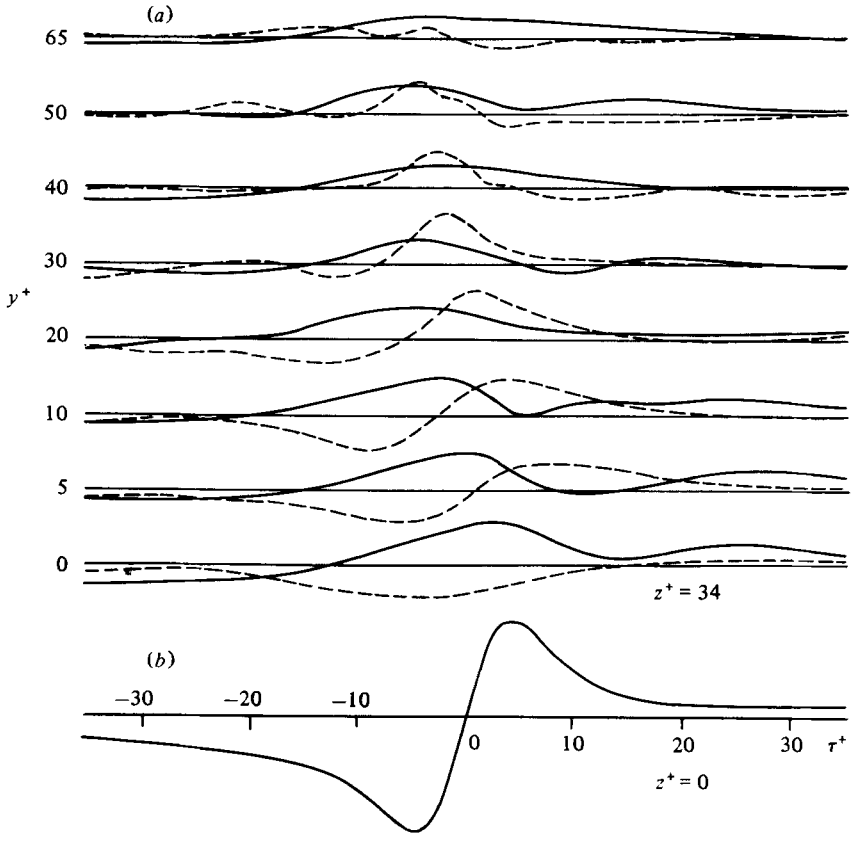

FIGURE 8. The same as figure 7 with $z^+ = 34$.

component is essentially negative over the entire $z^+ > 0$ range. This is consistent with the vortex model and arrangement of the sensors shown in figure 1 (*a*). Although not shown, $\langle(\partial w/\partial y)|_w\rangle$ were also measured at $z^+ < 0$ and were always antisymmetrical with respect to those at $z^+ > 0$, consistent with the vortex motion. After the sharp acceleration, the sweep arrives and the gradient of the streamwise velocity component is everywhere greater than its mean. In addition, the sweep is associated with a sign change of the gradient of the spanwise velocity component for $z^+ < 20$. This change occurs on the average before the sweep actually arrives at the wall location.

The conditional averages as a function of the normal distance from the wall obtained with the probe configuration shown in figure 1 (*b*) are found in figure 7 for $z^+ = 17$ and in figure 8 for $z^+ = 34$. In both cases the detection signal was obtained at $y^+ = 15$ and $z^+ = 0$ and the velocity scale is the same as in figure 6. The values shown at $y^+ = 0$ are the velocity gradients obtained from the wall elements. For orientation, the averages from the detector probe are shown at the bottom of each figure. In figure 7 one can clearly see the skewed nature of the sweep (as determined by the zero crossing of $\langle u\rangle$) as it arrives at various locations throughout the wall region. Before the sweep arrives, the conditional average of u is always less than its mean at $z^+ = 17$ and greater than its mean at $z^+ = 34$, consistent with the vortex motion. Prior to the sweep, the spanwise velocity component is negative at both z^+ locations and has a maximum magnitude of

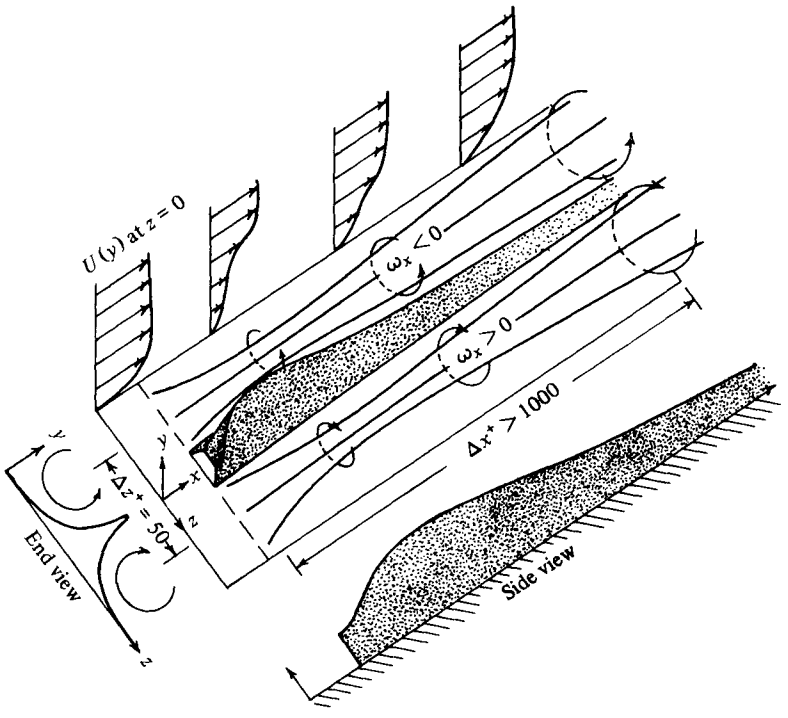

FIGURE 9. Model of the counter-rotating streamwise vortices together with the resulting low-speed streak. The velocity profiles are from Blackwelder & Kaplan (1976).

approximately 1 r.m.s. value at $y^+ = 10$ and $z^+ = 17$. Above $y^+ = 30$, the negative values of the spanwise velocity approach zero, indicating that the vortex structure is weaker and/or is more random at the higher elevations. The high-speed streamwise velocity associated with the sweeps is clearly seen at $z^+ = 17$. However, its effect is somewhat obscured at $z^+ = 34$ because of the already existing high-speed fluid due to the motion of the vortex system. As in figure 6, the spanwise velocity component is observed to change its sign almost everywhere slightly before the arrival of the sweep. It is interesting to note that, near the wall, the change of the sign of the spanwise velocity component leads that of the streamwise velocity component by 90°. This phase lead decreases at higher elevations and equals zero at $y^+ = 30$. The normalized spanwise velocity associated with the sweeps has large positive values everywhere, indicating that, near the wall, the sweep also has a three-dimensional character.

5. Discussion

Based upon these measurements, a model of the wall structure before the arrival of the sweep is shown in figure 9. Two counter-rotating streamwise vortices are represented by their corresponding vortex lines. These vortices exist in a region of a strong mean-velocity gradient; hence, between them, they 'pump' low-speed fluid away from the wall. This creates a low-speed streak illustrated by the shaded structure in the figure and an inflexional velocity profile. The vortices are quasi-periodic in the spanwise direction; hence regions of high-speed fluid also result at $z^+ = \frac{1}{2}\lambda_z^+$. This produces

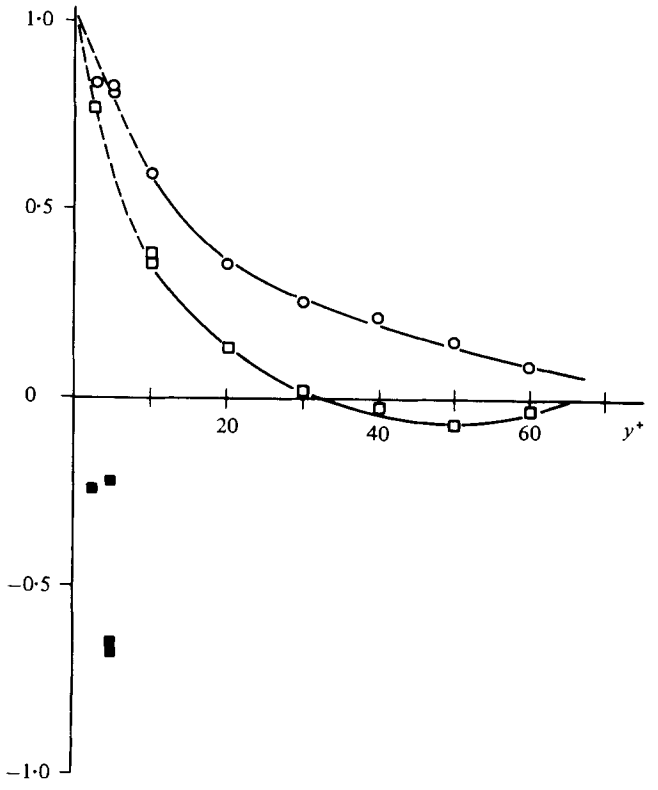

FIGURE 10. Spatial correlations with the separations normal to the wall: ○, $R_{w(\partial u/\partial y)}$; □, $R_{w(\partial w/\partial y)}$. The data associated with the probe interference are given by ■, $R_{w(\partial w/\partial y)}$.

a fuller velocity profile with greater stability and thus is probably not of great significance in the dynamics of the bursting phenomenon.

The detection criteria of Blackwelder & Kaplan (1976) was used to measure the streamwise and spanwise velocities as shown in figures 6–8. Examination of simultaneous signals and the data presented earlier indicate that their detection scheme triggered on the sharp acceleration associated with the abrupt ending of the low-speed streaks. The conditionally averaged velocity profiles of Blackwelder & Kaplan are thus associated with the streak and are sketched in the figure. These profiles at $z^+ = 0$ were essentially measured by passing through the low-speed streak from right to left, i.e. one first sees the profile as shown at the extreme right; a small inflexional region is seen as the low-speed region becomes larger followed by a strongly inflexional profile. After passing through the sharp acceleration, the full velocity profile associated with the sweep is seen at the left.

The spanwise wavelength of the vortex structure, λ_z, has been measured by Kim *et al.* (1971), Lee *et al.* (1974), and Oldaker & Tiederman (1977) using visualization techniques and by Gupta *et al.* (1971) using hot-wire probes. They all observed a skewed probability distribution of λ_z which had a most probable non-dimensional wavelength of $\lambda_z^+ = 80$ and an average wavelength of $\lambda_z^+ = 100$. This agrees with space–time correlations of the gradient of the spanwise velocities obtained by Blackwelder & Eckelmann (1978) and with the peak in the quadrant analysis in figures 3 and 5 of

$\Delta z^+ = 20$. The extent of the vortex structures normal to the wall is much more difficult to measure directly. The conditional averages shown in figures 7 and 8 indicate that the middle of the vortex structure lies at approximately $y^+ = 20$–30. However, this represents only an average position of a stochastic variable. Each vortex structure probably occupies a range of y^+ locations throughout its lifetime and this range varies from one vortex to another. The wall distance of $y^+ = 20$–30 is consistent with the correlation of the spanwise velocity components measured normal to the wall, as shown in figure 10, where a zero crossing is found at $y^+ = 30$. Because of the randomness associated with the structures, the centre of the vortex structure probably lies below that point. These estimates also agree with the data obtained by Gupta *et al.* (1971), Lee *et al.* (1974) and Kreplin (1976). The correlation of the streamwise velocity component as a function of the distance normal to the wall is also shown in figure 10. (Although a peculiar case of probe interference was observed for $y^+ < 10$ as discussed in the appendix, it does not affect the results stated here.)

The length of the streamwise vortices is difficult to estimate from the data reported here. By using space–time correlations of the streamwise and spanwise velocity gradients of the wall, Kreplin (1976) and Blackwelder & Eckelmann (1978) found correlations extending beyond $\Delta x^+ > 1000$. Motion pictures of this phenomenon taken by Oldaker & Tiederman (1977) indicate that streaks of dye lifted away from the wall can have scales in the streamwise direction of even greater lengths. However, the amalgamated dye streaks are only the result of a counter-rotating pair of vortices, and thus they do not necessarily yield a reliable estimate of the length of the vortices themselves.

The strength of these vortices can be estimated by using the conditionally averaged velocities obtained in figures 7 and 8. By assuming a typical diameter of $r^+ = 15$, their strength is approximately an order of magnitude less than the value of the spanwise vorticity measured at the wall.

The origin of the system of counter-rotating streamwise vortices is unknown. Similarly, it is difficult to explain exactly what happens to the vortices as the sweep arrives at the wall region. The vortex lines in figure 9 are shown to have an abrupt ending at the occurrence of the sweep, although it is known that this is not physically realizable. The conditional averages indicate that, as the sweep passes, high-speed fluid moves around the low-speed streak. This can be represented by a broad large-scale counter-rotating vortex system of the opposite sign to that shown in figure 9. Thus the vortex lines in the figure may either cross and/or be joined together with other vortices as the sweep arrives. This point requires further clarification.

The concluding picture is one of a pair of counter-rotating vortices of very long streamwise extent which pump fluid away from the wall to form a low-speed streak between them. This pumping action continues until it is interrupted by a sweep imposed by the outer flow field. The great length of the vortices in the streamwise direction tends to indicate that they are quasi-stable and hence are destroyed only by the action of the sweep. The high-speed fluid of the sweep flowing over the low-speed streaks forms the strongly inflexional velocity profile observed by Blackwelder & Kaplan (1976). The conditional averages of Wallace, Eckelmann & Brodkey (1972), Lu & Willmarth (1973), Blackwelder & Kaplan (1976) and others indicate that most of the turbulent energy is produced by the ejection from the wall of part of the low-speed streak and by its subsequent interaction with the incoming high-speed fluid. The

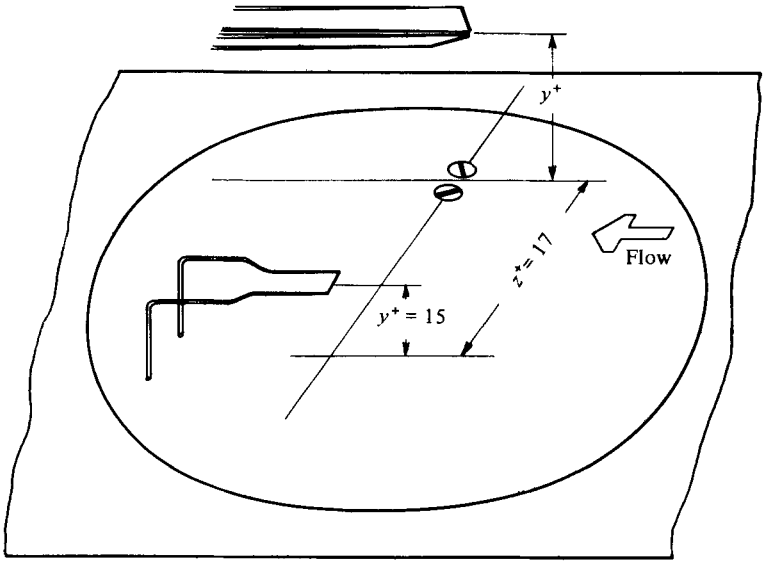

FIGURE 11. Sketch of the configuration used to check for probe interference.

ejection phase seems to be triggered by the sharp acceleration and inflexional profile which is associated with the outer flow field (Chen & Blackwelder 1978). Since the sweep of outer fluid triggers these events, the frequency of occurrence of the bursting phenomenon should scale with the outer flow variables, δ and U_∞, as observed by Narahari Rao, Narasimha & Badri Narayanan (1971). Thus the large-scale structures associated with the outer flow field play a dominant role in determining the break-up of the streaks. Some observations of the instantaneous signals in the present study suggest that the interaction between the high-speed sweep and the low-speed streaks can best be described as a localized free shear layer. Preliminary estimates of the thickness and velocity difference across the layer indicate that it is unstable and could be responsible for the regular oscillations that were observed at $y^+ \approx 15$ in some of the signals occurring with the sharp acceleration. A similar oscillation has been described by Kim *et al.* (1971). More work is required to clarify if this mechanism is indeed associated with the production of turbulent energy in the boundary layer.

This research was supported by the John S. Guggenheim Foundation and the Max-Planck-Institut für Strömungsforschung. Their assistance is gratefully acknowledged.

Appendix

Many precautions and checks were taken during this work to preclude the occurrence of any possible probe interference. However, it was observed that the correlation

$$R_{w(\partial w/\partial y)}(y^+) = \frac{\overline{w(y^+,t)\,\partial w(0,t)/\partial y|_w}}{\sqrt{(\overline{w^2}.\overline{(\partial w/\partial y)_w^2})}}$$

displayed a very irregular behaviour for $y^+ < 10$. In particular, very strong negative correlations were often obtained with separations of $y^+ = 5$ and less, as shown in

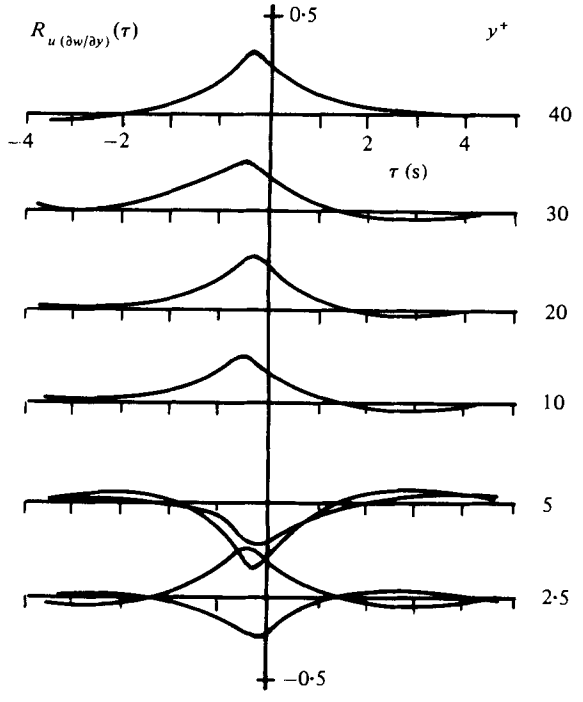

FIGURE 12. Space–time correlations of the streamwise velocity at $y^+ = 15$ and $z^+ = 0$ and the spanwise velocity gradient at $y^+ = 0$ and $z^+ = 17$. A third moveable probe was positioned at $z^+ = 17$ and traversed through the indicated y^+ positions.

figure 10. Since the signals themselves did not show any obvious errors, it was impossible to ascertain whether the flow field was being severely disturbed as the moving probe approached the wall. Thus in addition to the suspected correlations shown in figure 10, correlations between the streamwise velocity component at $y^+ = 15$ and $z^+ = 0$ and the gradient of the spanwise velocity component, $(\partial w/\partial y)|_w$, at $y^+ = 0$ and $z^+ = 17$ were computed as the V-probe directly above the wall elements approached the surface, i.e. $y^+ \to 0$ in figure 11. If no probe interference occurred, then

$$R_{u(\partial w/\partial y)}(y^+, z^+, \tau^+) = \frac{\overline{u(15, 0, t^+)\ \partial w(0, 17, t^+ + \tau^+)/\partial y|_w}}{\sqrt{(\overline{u^2}.\overline{(\partial w/\partial y)_w^2})}}$$

should remain constant for all values of the time delay because these sensors were fixed in space as the wall was approached by the other probe.

The results are seen in figure 12 for six different locations of the movable probe. As long as the V-probe was at $y^+ > 10$, the correlation function did indeed remain constant. At $y^+ = 5$, the correlation was observed to have approximately the same magnitude but an opposite sign. At $y^+ = 2{\cdot}5$, both a positive and negative correlation were obtained in two different attempts which could not be explained. Since the y^+ and z^+ separation would be determined within $\pm 0{\cdot}5$, such large differences in the correlations could not be attributed to positional errors. Whenever the correlation $R_{u(\partial w/\partial y)}(y^+, z^+, \tau^+)$ in figure 12 was negative, the correlation $R_{w(\partial w/\partial y)}(y^+)$ of figure 10 simultaneously yielded negative values. Further testing indicated that the signal

corresponding to the gradient of the spanwise velocity component at the wall suffered a 180° phase shift as the movable probe approached the wall. However, the signals and correlations of the gradient of the streamwise velocity component did not seem to be affected by the probe interference. By removing the electrical connexion to the movable probe, it was determined that the interference was not caused by electrical or thermal cross-coupling between the movable probe and the wall elements. The conclusion remained that the probe interference was indeed the result of the physical presence of the probe near the wall. Thus the movable probe seemed to cause a change in the existing structure and possibly imposed or promoted the existence of another structure in the wall area.

REFERENCES

BAKEWELL, H. P. & LUMLEY, J. L. 1967 *Phys. Fluids* **10**, 1880.

BLACKWELDER, R. F. 1977 *Phys. Fluids* **20**, S232.

BLACKWELDER, R. F. & KAPLAN, R. E. 1976 *J. Fluid Mech.* **76**, 89.

BLACKWELDER, R. F. & ECKELMANN, H. 1977 *Proc. EUROMECH* 90, *Nancy, France.*

BLACKWELDER, R. F. & ECKELMANN, H. 1978 *Structure and Mechanism of Turbulence*, Lecture Notes in Physics, p. 190. Springer.

CHEN, C. H. P. & BLACKWELDER, R. F. 1978 *J. Fluid Mech.* **89**, 1.

CORINO, E. R. & BRODKEY, R. S. 1969 *J. Fluid Mech.* **37**, 1.

CORRSIN, S. 1957 *Symp. Naval Hydrodyn., Publ.* 515, NAS-NRC 373.

ECKELMANN, H. 1974 *J. Fluid Mech.* **65**, 439.

GRANT, H. L. 1958 *J. Fluid Mech.* **4**, 149.

GUPTA, A. K., LAUFER, J. & KAPLAN, R. E. 1971 *J. Fluid Mech.* **50**, 493.

KIM, H. T., KLINE, S. J. & REYNOLDS, W. C. 1971 *J. Fluid Mech.* **50**, 133.

KLAGES, H. 1977 *Max-Planck-Institut für Strömungsforschung Bericht* 14/1977.

KLINE, S. J. & RUNDSTADLER, P. W. 1959 *J. Appl. Mech.* **E26**, 166.

KLINE, S. J., REYNOLDS, W. C., SCHRAUB, F. A. & RUNDSTADLER, P. W. 1967 *J. Fluid Mech.* **30**, 741.

KREPLIN, H. P. 1976 Experimentelle Untersuchungen der Langsschwankungen und der wandparallelen Querschwankungen der Geschwindigkeit in einer turbulenten Kanalströmung. Ph.D. thesis. Universität Göttingen.

LAUFER, J. 1975 *Ann. Rev. Fluid Mech.* **7**, 307.

LEE, M. K., ECKELMANN, L. D. & HANRATTY, T. J. 1974 *J. Fluid Mech.* **66**, 17.

LU, S. S. & WILLMARTH, W. W. 1973 *J. Fluid Mech.* **60**, 481.

NARAHARI RAO, K., NARASIMHA, R. & BADRI NARAYANAN, M. A. 1971 *J. Fluid Mech.* **54**, 39.

OLDAKER, D. K. & TIEDERMAN, W. G. 1977 *Phys. Fluids* **20**, S133.

SIRKAR, K. K. & HANRATTY, T. J. 1970 *J. Fluid Mech.* **44**, 605.

TOWNSEND, A. A. 1970 *J. Fluid Mech.* **41**, 13.

WALLACE, J. M., ECKELMANN, H. & BRODKEY, R. S. 1972 *J. Fluid Mech.* **54**, 39.

WILLMARTH, W. W. 1975 *Adv. Appl. Mech.* **15**, 159.